ELSEVIER

Journal of Biomechanics

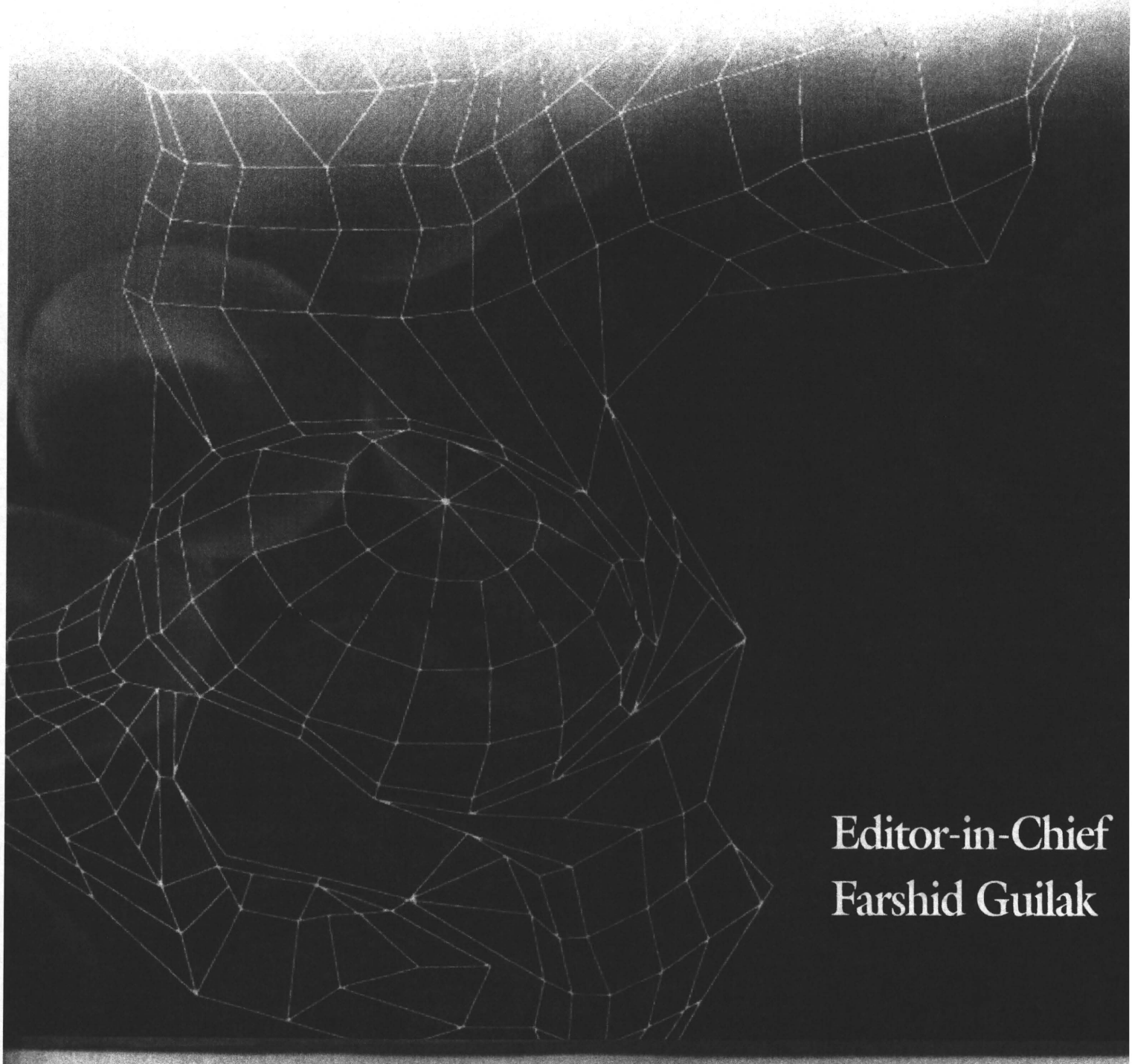

Editor-in-Chief
Farshid Guilak

different skill levels, gender and age, in different workspaces and in the presence of dynamic obstacles.

D-8
The Development of a Custom-made Intra-medullary Nail for Use in an Ovine Tibial Segmental Defect Model

A. Briscoe, A. Aarvold, M. Street, E. Tayton, J.O. Smith, D.G. Dunlop, R.O. Oreffo. *University of Southampton, UK*

The aim of this study was the development and manufacture of an intra-medullary nailing system to stabilise a tibial segmental defect in an ovine model, in order to study bone regeneration strategies. Tissue engineering is well established in orthopaedic research in vitro, and small animal studies have demonstrated the therapeutic effect of synthetic scaffolds seeded with mesenchymal stem cells in bone regeneration [1]. Upscaling to a large animal (ovine) model is necessary prior to translation to human clinical trials.

Difficulties in ovine models include strong and consistent methods of maintaining the critical bone defect in a fully weight bearing sheep. Potential methods are plating, external fixation or intra-medullary (IM) nailing, the latter two being the most clinically relevant. External fixation requires meticulous and labour-intensive post-operative care, thus the development of an intuitive, robust ovine IM device would be beneficial.

The breed of sheep selected, the Northern Mule, has a body mass up to 100 kg. The typical tibial medullary canal for this animal is 20 cm long and 8–9 mm in diameter. Reaming of the medullary canal affects the bone biology at the defect site which may confound results, therefore an oversized nail, though more stable, is undesirable for this model. The weakest points in the nail are the locking screw holes due to the removed material at these points and stress raisers. Increasing the nail diameter adds strength and an 8 mm diameter nail is the minimum possible diameter to accommodate holes for 3.5 mm diameter locking screws whilst maintaining enough strength to not buckle or bend over the defect length.

For human IM nail insertion, and previous ovine IM nail studies, distal locking screws are inserted freehand which requires intra-operative imaging. This adds time and expense to the procedure and increases personnel and equipment requirements and costs [2,3]. A jig was developed to align the drill and locking screws with the internal screw holes both proximally and distally. The novel insertion apparatus and technique presented in this paper consists of an external guide attached to the proximal end of the nail which is aligned with the screw holes and can be rotated and re-aligned with perpendicular holes allowing full locking of the nail within the bone.

This technique simplifies surgery and significantly reduces costs when compared to existing intra-medullary nailing systems.

Reference(s)

[1] Kanczler JM, Ginty PJ, White L, Clarke NM, Howdle SM, Shakesheff KM, Oreffo RO. The effect of the delivery of vascular endothelial growth factor and bone morphogenic protein-2 to osteoprogenitor cell populations on bone formation. Biomaterials. 2010 Feb;31(6):1242–50. Epub 2009 Nov 18.

[2] Stryker T2 Tibial Nailing System. Operative Technique. Literature number B1000005, LOT G3709. Copyright 2009.

[3] Reichert JC, Saifzadeh S, Wullschleger ME, Epari DR, Schütz MA, Duda GN, Schell H, van Griensven M, Redl H, Hutmacher DW. The challenge of establishing preclinical models for segmental bone defect research. Biomaterials. 2009 Apr;30(12):2149–63. Epub 2009 Feb 10. Review.

D-9
Interpositional Knee Devices: The Way Forward?

T. Akram[1], F. Brooks[1], A. Chandratreya[1], S. Roy[2], D. Pemberton[2]. [1]*Princess of Wales Hospital, Wales;* [2]*Royal Glamorgan Hospital, Llantristant, Wales*

Osteoarthritis is the most common progressive degenerative disorder of the cartilage of joints. Treatment of osteoarthritis (OA) is evolving, allowing the Orthopaedic surgeon and patient more options including the choice of surgical intervention at an earlier stage of the disease. The interpositional knee device is a recently developed patient specific implant used for the treatment of uni-compartmental OA and the correction of leg axis deformity. It is designed for use in mild to moderate osteo-arthritis only. It offers benefits over the traditional surgical management methods of uni-compartmental OA. It is less invasive, can be performed as a day procedure and does not limit future options. The National Institute for Clinical Excellence (NICE) recently issued guidance on the use of this device as experimental.

A young adult with uni-compartmental arthritis is suitable for this implant instead of a uni-compartmental knee replacement or a high tibial osteotomy. A Magnetic Resonance Imaging (MRI) scan of the patient's knee is reviewed by the local radiologists along with a radiologist in the US to decide if the patient is suitable for the implant based on a number of factors. A bespoke implant, based on the MRI data, is produced. Prior to insertion of the device an arthroscopic procedure is undertaken to allow proper positioning of the implant in the knee.

We have treated 26 patients with the iForma Conformis interpositional knee implant in South Wales at the Princess of Wales Hospital, Bridgend and the Royal Glamorgan Hospital, Llantrisant since November 2007. The pre- and post-operative Western Ontario and McMaster Universities (WOMAC) Osteoarthritis Index scores were recorded prior to surgery and at the last follow up appointment. The average age was 54.7 years, Body Mass Index (BMI) 32; there were 9 females and 17 males. The average pre-operative WOMAC score was 42.2 with an improvement to 62.9 post-operatively. A total of 33 implants were used (20 right, 13 left). Only 5 lateral compartment implants were used. 7 patients experienced post-operative problems (5 implants removed and 2 MUAs). No dislocations were reported. The average follow-up time was 19.2 months (range 10–27 months).

Our early experience suggests patient selection plays a vital role in the outcome of patients following surgery. It indicates that the interpositional knee device is a viable and safe alternative to a uni-compartmental knee replacement. A further study is underway to compare this procedure with the uni-compartmental knee device.

D-10
A Navigated Unilateral External Fixation System for Deformity Correction Incorporating Preoperative Surgical Simulation and Intraoperative Razor Guidance

I. Ohnishi, T. Matsumoto, M. Bessho, S. Ohashi, K. Tobita, M. Kaneko, K. Nakamura. *University of Tokyo, Japan*

Ring frames like Ilizarov or Taylor Spatial Frame[1] are preferred for correction of severe and complex multi-plane deformities. However, the available frames are heavy and bulky leading to poor compliance by patients. Also, the mounting procedure requires considerable expertise and skill, and it is technically demanding to insert penetrating wires for application to the proximal femur. On the other hand, a unilateral external fixator has the advantages of less bulk and a lighter weight. Thus, it causes less disability and can achieve better patient compliance even with bilateral application. However, previous unilateral fixators have had various limitations with respect to deformity correction, such as restricted placement of hinges, restricted correction planes, and a limited range of correction angles. In addition, it was impossible to achieve progressive correction while fixation was maintained. To overcome these disadvantages of existing unilateral fixators, a new unilateral external fixator with a universal bar link system has been developed that can achieve acute and gradual correction of multi-plane deformities, including rotational and translational deformities.

Preoperative surgical planning for determining optimal mounting of the fixator is performed using a 3D STL model of the bone created from preoperative CT scans and CAD data of the fixator. A correction

hinge can be placed exactly right on the centre of rotational angulation (CORA) or at any desired location with the preoperative planning. Virtual deformity correction can be performed and final outcome after correction can be assured in 3D plane.

A laser-beam projection system has been developed, which allows us to obtain surgical guidance information. Utilizing the system, pin insertion sites and direction as well as placement of the fixator can be determined intraoperatively as exactly as preoperatively planned. Laser beams are directly projected onto the surgical field so that the surgeons are able to obtain accurate guidance information. Two laser-beam lines are projected onto the cylindrical tool surface. When two beams align parallel, precise insertion of the tool can be done as previously planned. With this guidance system, we don't have to look at a monitor to make sure that insertion direction is precise or not. We are able to just keep on looking at the devices we hold.

Gradual correction of the deformity can be performed by rotating three dials mounted on the link using a warm geared goniometer that is temporarily attached to the apparatus, while fixation is maintained. The fixator is manipulated by rotating each of the three dials to the predetermined angles calculated by computer software. The goal of treatment is to restore physiological orientation of the knee and ankle joints, as well as to restore physiological alignment of the mechanical axis.

Mechanical testing demonstrated that this new fixator had sufficient strength for full weight bearing as well as sufficient fatigue resistance for repeated or prolonged use. The results of clinical application in patients with multi-plane femoral deformities were excellent, and correction with very small residual deformity was achieved in each plane.

Reference(s)

[1] Taylor JC: Perioperative planning for two- and three-plane deformities. Foot & Ankle Clinics. 13(1): 69–121, 2008

D-11
A Combined Passive and Active Joints Robotic System for Photodynamic Therapy for Port Wine Stains

G. Bian[1], Q. Huang[1], X. Duan[1], H. Li[1], X. Wang[1], H. Zhao[1], Y. Gu[2]. [1]*Intelligent Robotics Institute, Beijing Institute of Technology, China;* [2]*Chinese People Liberation Army General Hospital, China*

Port Wine Stain (PWS) birthmarks are congenital vascular malformations, which usually appear at birth and tend to become darker and thicker with age's growth. Vascular-targeted Photodynamic Therapy (PDT) is an effective approach among the treatments for PWS. However, due to the arbitrariness of manual operation and pole points existing in laser radiation, the PWS zone was always cured unevenly in clinics. This paper presents a novel robotic system, which consists of a passive arm and an active wrist, for assisting doctors to exert PDT treatments. In clinics, compared to the fully actuated robot, the passive arm is more convenient and safer to be operated; the two Degrees of Freedom (DOFs) active wrist can automate PDT under the guidance of binocular vision, so the doctors can focus more concentration on clinical judgments and treatments rather than do heavy manual work. The workflow to use the robotic system is as follows. In pre-treatment, the doctor should firstly adjust the passive arm to an appropriate pose (position and orientation), after that the robotic system should acquire enough images around the lesion by the binocular vision, and then the doctor could segment the lesion easily on a Liquid Crystal Display (LCD) panel with a mouse, finally the workstation could reconstruct the lesion's 3-Dimensional (3-D) models with surface rendering method. During the treatment, based on the 3-D positions of the boundary of the lesion, the workstation will manipulate the active wrist to move the laser tip according to the doctor's setting. This paper, firstly, introduced the mechanism of PWS and its treatments. Based on the prosperities of PDT, we designed the robotic system architecture, which consists of the medical robot, binocular vision and workstation. Then the detailed mechanical design on the robot with combined passive and active joints was given. The passive arm has four joints, each of which has a built-in electromagnetic brake, which can lock the joint at any angle during the treatment and loose it by pushing an electrical button when needed to revolute. The active wrist has two joints, which can automatically manipulate the laser tip in PDT. Furthermore, we discussed the kinematic analysis and uniform radiation, which is the key direct factor for PDT. To validate the robotic system, we have done three experiments to assess the accuracy respectively on the robot, the binocular vision and the whole robotic system. Experimental results showed that the robotic system could reduce much more work burden and realize more uniform radiation than manual work could. The clinical results will be given after the accomplishment of the ongoing clinical experiments. Obviously, this robotic system can also be employed in other laser-based therapy for uniform radiation.

D-12
Mechanism Design Issues for Minimally Invasive Surgical Robots

C.H. Kuo[1], J.S. Dai[1], P. Dasgupta[2]. [1]*King's College London, UK;* [2]*Guy's and St Thomas' Hospitals NHS Foundation Trust, UK*

Introduction and Objectives: Design of minimally invasive surgical (MIS) robots is a great challenge because it involves multiple specialties spread in the fields of medicine and engineering. From the engineering side, the robot design can be further managed into various aspects such as the manipulator design, actuation strategy, motion control, vision acquisition and processing, etc. Among the various specialties, mechanism design plays a predominated role in the whole design process; however, there is still no literature dedicated to the mechanism design of MIS robots. This paper, therefore, aims at providing a figure to the mechanism design of MIS robots.

Material and Methods: Based on the exhaustive review of the literatures in MIS robot design, the challenges for mechanism design of MIS robots are studied. First, an exclusive kinematic feature in MIS robots, namely "remote center-of-motion (RCM)", is revisited. Secondly, the design issues for mechanism design of MIS robots are discussed.

Results: A general mechanism design procedure for MIS robots is summarized. Accordingly, eleven design issues for the mechanism design of MIS robots, including the RCM function, ergonomics, kinematic redundancy, backdrivability, modularity, safety, accuracy, workspace, dexterity, singularity, and isotropy, are concluded.

Conclusions: As a result, this paper provides a comprehensive overview to the mechanism design of robotic manipulators used for minimally invasive surgery. It suggests researchers a way to follow-up when designing the manipulator structure of MIS robots. It contributes to both mechanisms and medical communities for the kinematic analysis and mechanism design of MIS robots.

D-13
A Metamorphic Instrumental Hand for Robot Assisted Minimally Invasive Surgery

H. Luo, S. Wang. *Tianjin University, China*

Instrumental hands for robot assisted minimally invasive surgery (MIS) perform surgical operation inside the abdomen of the patient under a surgeon's control. In this paper, a three-fingered metamorphic instrumental hand derived from the planar four bar mechanism is proposed for the robot assisted MIS. The metamorphic instrumental hand is aimed to improve the robot assisted MIS manipulation. It is composed of one metamorphic mechanism and three independent operational fingers. The metamorphic mechanism is capable of changing the topological structure of the device from a pole to a three fingered instrumental hand during operation, and return to a pole again after operation. The metamorphic characteristic enables the instrumental hand to


ORS
Orthopaedic Research Society
Transactions
Abstracts
Program
Copyright
Help
2011 Annual Meeting of the
Orthopaedic Research Society
January 13-16, 2011
Long Beach Convention Center • Long Beach, California

Measurement of Articular Cartilage Thickness Using a 3D Image Reconstructed from B-mode Ultrasonography Mechanical Scans -Comparison with MRI-derived Data-

[1]Ohashi, S; +[1]Ohnishi, I; [1]Matsumoto, T; [1]Bessho, M; [1]Matsuyama, J; [1]Tobita, K; [1]Kaneko M; [1]Nakamura, K
+[1]Department of Orthopaedic Surgery, Faculty of Medicine, University of Tokyo, Tokyo, Japan
ohnishii-dis@h.u-tokyo.ac.jp

INTRODUCTION

Although articular cartilage thickness has previously been quantified using B-mode ultrasonography (US) [1, 2], thicknesses in those studies were measured 2-dimensionally using B-mode slice images. Cartilage thickness has also been quantified by creation of 3-dimensional (3D) models from MRI data [3, 4], but this approach has not been adapted to US. The purpose of this study was to develop a method to measure 3D articular cartilage thickness at the femoral condyle using B-mode US and to compare results with 3D measurements using MRI to clarify the feasibility of US in clinical evaluations of articular cartilage.

OBJECTIVES AND METHODS

US B-mode image acquisition

Subjects comprised 2 healthy male volunteers (age, 37 and 59 years) and 2 male patients with knee osteoarthritis (age, 73 and 81 years) who provided written informed consent prior to participation in the study. The study protocol was approved by the ethics committee of our institution. A B-mode 10.0-MHz linear ultrasound probe (UST-5411; Aloka, Tokyo, Japan) connected to an ultrasound device (Prosound ALPHA 10; Aloka) was attached to a probe scanner stabilized by a holding arm, allowing the ultrasound probe to move along the surface of the flexed knee (Fig. 1A). The base of the holding arm was rotated by a gear and data on angle of rotation of the arm was transferred to the ultrasound device by an encoder. Scans with angle data were recorded. The medial surface of the right knee of each participant was scanned using the ultrasound probe with the knee flexed at 120° (Fig. 1B) so the cartilage surface of the femoral medial condyle could be visualized by US. The US probe was attached to the arm so the US imaging plane was parallel to the arm plane, allowing the imaging plane to rotate around the center axis of the encoder, which was coaxial with the medial-lateral axis of the femoral condyle. The range of the angle of rotation for the arm was 0-80° and the US B-mode images (total, 101 images) were acquired every 0.8° (Fig. 2A). System settings were optimized to image the cartilage surface (tissue harmonic, 420 pixels × 468 pixels; pixel size, 0.0855 mm × 0.0855 mm).

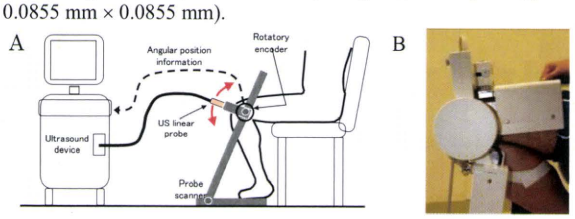

Figure 1. A) Illustration of the entire US system for knee cartilage image acquisition. **B)** Side view of a knee in the probe scanner.

Cartilage area extraction and 3D model creation (US and MRI)

Image and position data were imported to the originally developed software and slice images were aligned in 3D in the proper position (Fig. 2B, C). Parallel slice images were then created using the multiple plane reconstruction method and imported to the 3D model creation software (Mimics; Materialize, Leuven, Belgium). Cartilage area was extracted in each image using the Livewire method of the software [5] and a 3D cartilage model was created from the extracted cartilage area. MR images of the knees were acquired using the sequence previously described [4] from the MRI device (Achieva 3.0T X-series; Philips, Eindhoven, the Netherlands; 512 pixels × 512 pixels; pixel size, 0.313 mm × 0.313 mm; slice thickness, 0.600 mm; slice gap, 0.291 mm). DICOM data from MRI were imported to Mimics and a 3D cartilage model was created after extraction of cartilage area in each image as similarly done for US.

Articular cartilage thickness comparison

The 3D data for 3D cartilage models from US and MRI were imported to 3D inspection software (Rapidform XOV; INUS Technology, Seoul, Korea) and aligned using the point registration method (Fig. 3C). Cartilage thickness (Tc) in each model was visualized by color mapping (Fig. 3A, B). Cartilage thickness was determined at 400 points 1 mm apart from one another in the US model (Tc-US) and the MRI model (Tc-MRI). Linear regression analysis was performed and Pearson's coefficient of correlation was used to compare Tc-US with Tc-MRI. A correlation was considered significant for values of $p<0.05$.

Figure 2. A) Original B-mode US image of a participant knee. **B)** US image of the knee from the side, reconstructed from original US images in A). **C)** Illustration of US image alignment. Original US images in A) were aligned three dimensionally in the proper position.

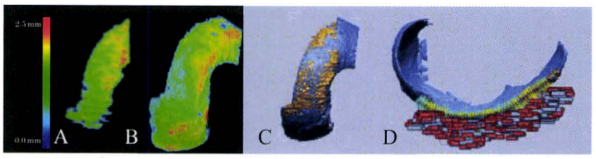

Figure 3. Color mapping of cartilage thickness with the 3D US model **(A)** and the 3D MRI model **(B)**. **C)** The 3D US and MRI models were aligned by point registration. **D)** Cartilage thickness measurements from both models at 400 points 1 mm apart from one another.

RESULTS

With color mapping of articular cartilage thickness, the US model exhibited relatively good similarity to the MRI model in thickness distribution (Fig. 3A, B). Tc-US correlated significantly with Tc-MRI in all participants ($p<0.0001$, each) (Fig. 4). Pearson's coefficient of correlation tended to be slightly higher in volunteers than in patients with osteoarthritis.

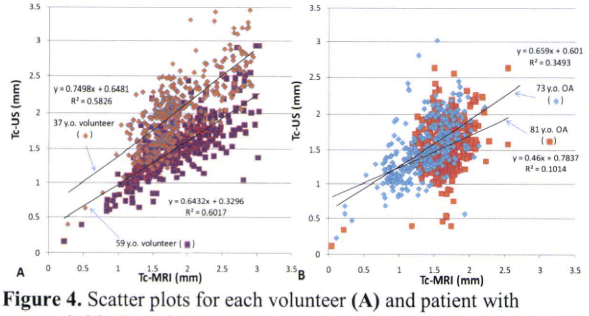

Figure 4. Scatter plots for each volunteer **(A)** and patient with osteoarthritis **(B)**. Linear regression analysis shows good agreement between Tc-US and Tc-MRI in all plots. OA: osteoarthritis.

DISCUSSION

This is the first study to clinically measure Tc using a 3D US cartilage model, although 3D US has been adopted for evaluating other tissues, such as the Achilles tendon [6] and rotator cuff [7].Considering the high accuracy of Tc measurement using MRI [8], our results show that, like MRI, Tc-US measurement using 3D models also allow accurate measurement of Tc, in both healthy individuals and patients with osteoarthritis.

REFERENCES

[1] Myers et al. J Rheumatology, 1995; 22: 109-16.
[2] Burkhard et al. Arthritis & Rheumatism, 2009; 61: 435-41.
[3] Eckstein et al. Osteoarthritis Cartilage, 2007; 15: 1326-32
[4] Eckstein et al. Ann Rheum Dis, 2006; 65: 433-41
[5] Bowers et al. Osteoarthritis Cartilage, 2008; 16: 1167-73
[6] Iagnocco et al. Clin Exp Rheumatol, 2009; 27: 547-51
[7] Kang et al. Skeletal Radiol, 2009; 38: 1063-9
[8] Burgkart et al. Arthritis & Rheumatism, 2001; 44: 2072-7.

ACKNOWLEDGEMENT

This work was funded by a grant-in-aid for Comprehensive Research on Aging and Health H19-007 from the Health and Labour Sciences Research Grants from the Ministry of Health, Labour and Welfare of Japan.

Effect of low-intensity pulsed ultrasound stimulation on callus remodeling in a gap healing model - Evaluation by bone morphometry using 3-dimensional quantitative micro computed tomography -

[1]Tobita, K; +[1]Ohnishi, I; [1]Matsumoto, T; [1]Ohashi, S; [1]Bessho, M; [1]Kaneko M; [1]Matsuyama, J; [1]Nakamura, K
+[1] Department of Orthopaedic Surgery, Faculty of Medicine, University of Tokyo, Tokyo, Japan
ohnishii-dis@h.u-tokyo.ac.jp

INTRODUCTION

Low-intensity pulsed ultrasound stimulation (LIPUS) effects are reportedly derived from the promotion of cell differentiation, which induces acceleration of fracture healing, resulting in earlier restoration of strength at the fracture healing site.

Previous studies have attempted to determine which stages of fracture healing are affected by LIPUS. Many basic studies suggested that LIPUS affected the inflammation, angiogenesis and soft callus formation stages. However, several studies suggested that LIPUS had no promoting effect in hard callus formation and remodeling stages [1]. Most previous basic studies have investigated the effects of LIPUS by histological evaluation, which is useful in clarifying cell differentiation and the formation of tissue morphology/arrangement, but is limited to observation in a 2-dimensional (2D) plane. Another method adopted has been mechanical testing of harvested specimens, but this is limited in that the testing is destructive and the strength of the healing site is evaluated in only one of multiple spatial planes.

In recent years, several basic studies have investigated fracture healing site morphology using micro-computed tomography (μCT). The advantage of μCT lies in the non-destructive morphological and densitometric assessments in 3-dimensional (3D) planes. In evaluating the effects of LIPUS on fracture healing by means of μCT, assessment is only possible after the healing stage has formed mineralized fracture callus.

The purpose of the present study was to quantitatively evaluate the effect of LIPUS on bone healing by means of μCT throughout both modeling and remodeling processes using a gap healing model in rabbits.

MATERIALS AND METHODS

Surgical Procedures

A total of 42 skeletally mature between 21 and 23-week-old male Japanese white rabbits (Kitayama Labes, Nagano, Japan), weighing 3.4-4.0 kg, were used for this study. Under general anesthesia, four transfixation pins (diameter, 2 mm; length, 50 mm) were inserted at the metaphyseal regions of the tibia in the frontal plane using a custom-made surgical pin driver. Transverse osteotomy was performed using a T-saw (blade thickness, 0.36 mm) with continuous irrigation with saline solution across the mid-shaft of the tibia at 12 mm distal to the tibio-fibular junction. The osteotomy with a 2-mm gap was immobilized with four pins fixed to an external fixator with double side bars. All procedures were performed in accordance with the guidelines of the Association for Assessment and Accreditation of Laboratory Animal Care (AAALAC).

LIPUS Treatment

The LIPUS system (model SAFHS®2000J, Teijin Pharma, Tokyo, Japan), which transmits 200-μsec burst of 1.5-MHz sine waves repeated at 1kHz with an average intensity of 30mW/cm^2, was used. After postoperative day 3, LIPUS was continued under general anesthesia for both the treatment group (n=7/group/time point) and the control group (n=7/group/time point). The transducer was placed onto the anterior surface of the operated leg with ultrasound coupling gel, for 20 min, six times/week, for 4, 6, or 8 weeks. The control group also received a sham inactive transducer under exactly the same condition as the LIPUS group.

μCT Analysis

All animals were euthanized with CO_2 asphyxiation and the entire right tibia was removed. After removal of soft tissues, the harvested tibia was scanned by μCT (Scan X mate-E090; Comscantecno, Kanagawa, Japan). The scan was performed along the long axis of the diaphysis, with a voltage of 60 kVp and a current of 80 μA. Scan range covered 5 mm proximal and 5 mm distal to the center of the gap, with a resolution of 28.57 μm^3 voxel size. The region of interest (ROI) was set at the callus healing area (Fig. 1) defined by the gap filled with callus in 2D-CT scans and extended 0.5 mm proximally and distally from the center of the osteotomy gap with a total of 36 CT axial scans. 3D reconstruction of mineralized tissue was performed using a TRI-BONE system (Ratoc System Engineering, Tokyo, Japan). A threshold for newly formed mineralized callus was set as 200 mg/cm^3 [2].

Morphometric parameters used for evaluation were mineralized callus volume (BV, cm^3) and volumetric bone mineral density of mineralized tissue comprising the callus (mBMD, mBMD = BMC/BV, mgHA/cm^3). The whole ROI was measured and was subdivided into three zones (Fig. 1): a periosteal callus zone (External; red zone); a medullary callus zone (Endosteal; green zone); and the cortical gap zone as the remaining zone (Intercortical: yellow zone). For each zone, BV and mBMD were measured.

Statistical Analysis

The μCT evaluations were analyzed using a one-way ANOVA test. If that correction did not achieve normality, then a Kruskall-Wallis ANOVA on ranks was utilized. Data were all presented in mean and standard error of the estimate. Values of $p<0.05$ were considered statistically significant.

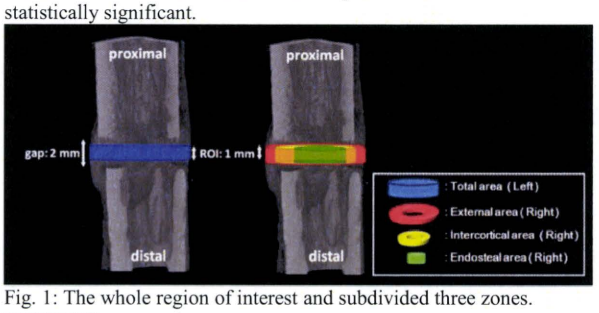

Fig. 1: The whole region of interest and subdivided three zones.

RESULTS

Callus Volume

The results of BV were shown in Fig.2. The control groups showed no significant differences. However, in the LIPUS groups, mean BV for the Endosteal zone was significantly lower for the 8-week group than for the 4-week group ($p < 0.05$). Comparing results at the same time point, the LIPUS group at 8 weeks was significantly higher than that of the control group in the Intercortical zone ($p<0.001$).

Volumetric Bone Mineral Density of Mineralized Tissue

The results of mBMD were shown in Fig. 3. The control groups showed no significant differences. However, in the LIPUS groups, the 8-week group was significantly higher than the 4-week group for Total, External, Internal, and Endosteal zones, respectively ($p < 0.001$, 0.001, 0.001, and 0.05). Comparing results at the same time point, the LIPUS group at 8 weeks was significantly higher than that of the control group in both External ($p < 0.05$) and Intercortical ($p < 0.05$) zones.

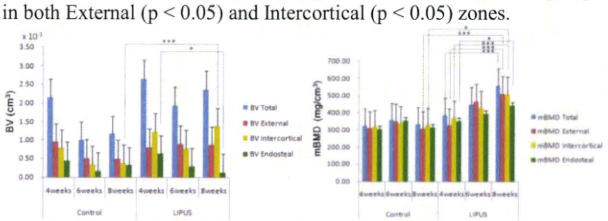

Fig.2-3: The result of BV (left) and mBMD (right) were showed. *= $p < 0.05$, ***= $p < 0.001$

DISCUSSION

The current investigation focused on the morphology of the gap healing site under the influence of LIPUS by quantifying changes in the localization of newly formed callus. The most striking finding in our study was that LIPUS accelerated bone formation in the External and Intercortical zones and callus resorption in the Endosteal zone. Therefore, LIPUS enhanced corticalization and medullary canal formation at the gap healing model, which could lead to earlier restoration of the structural integrity of the healing site.

REFRENCES

1. Claes L et al, *Prog Biophys Mol Biol*, 93, 2007
2. Augat P et al. *Calcif Tissue Int*, 60, 1997

ACKNOWLEDGEMENT

This project was supported by Teijin Pharma Limited, Tokyo, Japan.

CT-based finite element method for predicting the strength of the proximal femur in patients with postmenopausal osteoporosis
- Evaluation of inter- and intra-observer reliabilities and reproducibility -

+*Bessho, M; *Ohnishi, I; *Kaneko, M; *Matsumoto, T; *Ohashi, S; *Tobita, K; *Nakamura, K
+*Department of Orthopaedic Surgery, University of Tokyo, Tokyo, Japan
email: ohnishii-dis@ h.u-tokyo.ac.jp

Introduction:

The increase in fragility fractures of the proximal femur has become one of the major problems of an aging society. It has now become much more significant to accurately assess fracture risk and to establish effective prevention strategies in each individual osteoporotic patient.

Clinically available methods for estimating bone strength include bone densitometry, such as DXA (dual energy X-ray absorptiometry) or pQCT (peripheral quantitative computed tomography), and imaging modalities, such as X-ray or CT. Such techniques evaluate regional bone density and morphology, which are partly related to fracture risk, but they are of limited value for quantifying structural strength [1, 2]. Therefore, it is necessary to develop a noninvasive method to accurately quantify bone strength, incorporating information on the three-dimensional distribution of morphology, density, and material properties.

We established a quantitative computed tomography (QCT)-based finite element method (QCT/FEM) that was able to more accurately quantify the structural strength of the proximal femur than previous methods [3].

QCT/FEM must have a high accuracy and reproducibility if it is to be repeatedly used in longitudinal clinical studies. Therefore, the purpose of this study was to investigate the inter- and intra-observer reliabilities of the analysis of the strength of the proximal femur in patients with postmenopausal osteoporosis. Moreover, the reproducibility of the method was also evaluated by repeated analyses of a fresh cadaver specimen of the proximal femur.

Materials and Methods:

The study protocol was approved by our ethics committee, and the patients were enrolled after giving their informed consent. Axial CT scans of the proximal right femur were obtained in 12 female patients (mean age, 78 years) with postmenopausal osteoporosis (Aquilion Super 4, Toshiba Medical Systems Co., Tokyo, Japan; 120 kVp, 75 mAs, 512×512 matrix, pixel spacing 0.683 mm, slice thickness 3 mm), as well as scans of a calibration phantom.

A right femur with no skeletal pathology was collected within 24 hours of death from a 72-year-old female. A bone specimen was stored at -70 °C after each step of the protocol. The specimen was trimmed with a handsaw 14 cm distal to the midpoint of the lesser trochanter, and the proximal part was used for the experiments. After thawing, the trimmed specimen was cleaned of all soft tissues [1]. The specimen was then immersed in water, and axial CT scans were obtained with a slice thickness of 3 mm and a pixel width of 0.625 mm using the Aquilion Super 4 (Toshiba Medical Systems Co.; 120 kVp, 75 mAs, 512×512 matrix), as well as a calibration phantom. Repeated QCT scans were performed with repositioning of the specimen, and 6 data sets were obtained for analyzing reproducibility.

From the QCT data, FE models were created using triangular shell elements with a thickness of 0.4 mm and a size of 3 mm for the outer surface of the cortical bone and tetrahedral solid elements with a size of 3 mm for the rest of the bone [3]. To allow for bone heterogeneity, the mechanical properties of each element were computed from the Hounsfield unit value. Ash density for each voxel was determined from the linear regression equation derived by relating the Hounsfield unit of a calibration phantom to the equivalent ash density. Young's modulus and the yield stress of each tetrahedral element were calculated using the equations proposed by Keyak et al. [4] and Keller [5]. Poisson's ratio for each element was set at 0.4. Boundary conditions were applied to this model to represent the stance configuration [4, 6]. Materially nonlinear FE analysis was performed using the Newton-Raphson method. The predicted fracture load of the proximal femur was defined as the load causing failure of at least one shell element [3].

Two orthopedic surgeons (Observers A and B) independently analyzed strength from the same data of the proximal femur for each patient. According to the method of Feldman, each observer analyzed the same data twice [7]. The time interval between the first and second analyses was more than 3 weeks. Intra-class correlation (ICC) coefficients were used as indices for inter- and intra-observer reliabilities. From the strength data acquired by Observer A, with scans and analyses of the proximal femur specimen repeated six times, the coefficient of variation was calculated.

Results:

Strength data analyzed by Observers A and B are shown on Table 1. There was no significant difference in the mean analyzed strength between the first and second analyses for Observer A ($p = 0.591$). Likewise, there was no significant difference for Observer B ($p = 0.259$). In addition, there was no significant difference in the mean analyzed strength between Observers A and B ($p = 0.917$). Intra-observer reliability as assessed by the intra-class correlation coefficient was 0.924 for Observer A and 0.956 for Observer B. Inter-observer reliability as assessed by the intra-class correlation coefficient was 0.905. The mean analyzed strength and the standard deviation of the specimen for the repeated analyses were 3675 N and 52.4 N, respectively. Reproducibility as assessed by the coefficient of variation was 1.43%.

Table 1: Analyzed strengths by Observers A and B (N)

Observer A

	First trial		Second trial	
	M	SD	M	SD
Predicted Fracture Load (N)	4390	320	4365	380

Observer B

	First trial		Second trial	
	M	SD	M	SD
Predicted Fracture Load (N)	4385	370	4345	350

M: mean, SD: Standard Deviation

Discussion:

Altman et al. classified reliability as assessed by the ICC coefficient as good with a coefficient of 0.61-0.81 and as very good with a coefficient of 0.81-1.00 [8]. Therefore, the reliability of our method was considered to be very good. Cody et al. reported that the reproducibility of their QCT/FEM was 1.85% from repeated analyses of the QCT scans from 10 volunteers [9]. The result for the reproducibility of our method appears to be nearly identical. The reproducibility of DXA for the proximal femur has been reported to be 2-3% [10]; the reproducibility of QCT/FEM can attain the same level. In conclusion, QCT/FEM can be used in a longitudinal cohort study investigating the change in strength analyzed over time.

References:

[1] Cody, D.D., et al., J Biomech, 1999. 32(10): p. 1013-20.
[2] Faulkner, K.G., et al., Osteoporos Int, 1993. 3(1): p. 36-42.
[3] Bessho, M., et al., J Biomech, 2007. 40(8): p. 1745-53.
[4] Keyak, J.H., et al., J Biomech, 1998. 31(2): p. 125-33.
[5] Keller, T.S., J Biomech, 1994. 27(9): p. 1159-68.
[6] Bessho, M., et al., Bone, 2009. 45(2): p. 226-31.
[7] Feldman, D.S., et al., J Pediatr Orthop, 2007. 27(2): p. 204-8.
[8] Altman, D.G., Practical Statistics for Medical Research. 1991, New York: Chapman and Hall.
[9].Cody, D.D., et al., Ann Biomed Eng, 2000. 28(4): p. 408-14.
[10].Adams, J.E., Eur J Radiol, 2009. 71(3): p. 415-24.

11th EFORT Congress - 47 Congreso SECOT | Madrid | 2-5 June 2010

Congress Info | Social | Scientific | Registration | Exhibition & Sponsorship

Home | EFORT Homepage | SECOT Homepage | Contact information | Top contacts

REGISTRATION | ABSTRACT SUBMISSION

Congress and social

Dear Participant,

The 11th EFORT Congress will be held in association with the Spanish Orthopaedic and Traumatology Society (SECOT), thereby combining two major European events in our specialty.

- Schedule at a glance
- Congress deadlines

Scientific

Access restricted for Faculty only.
Please log on with your code here:

Username:

Password:

OK

* Request your access code at:
event@efort.org

NEW: Final programme

Exhibition

Dear Industry Partner,

Welcome to the EFORT Congress 2010 in Madrid, Spain to meet your important customers, share experience and build up awareness of future trends.

The EFORT team invites you to log on to the industry private section below and access the Exhibitor and Sponsoring Manual.

Name of the Company:

Access code:

OK

* *Request your access code at* sponsor@efort.org

CeramTec
THE CERAMIC EXPERTS

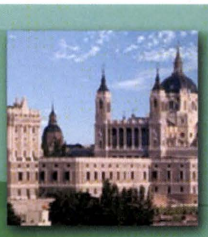

47º Congreso SECOT
Sociedad Española de Cirugía Ortopédica y Traumatología

11th Congress EFORT
European Federation of National Associations of Orthopaedics and Traumatology

MADRID, SPAIN 2 - 5 June 2010

Free Papers
E-Poster
Symposia
Instructional Lecture
Controversial Case Discussions
Guest Societies
ExMEx
Comprehensive Review Course
Satellite Symposia
Plenary Sessions
Comunicaciones SECOT
E-Poster SECOT
Sesiones SECOT
Index of Authors
Timetable
Search

Free Paper Content CLOSE SESSION

General Orthopaedic/complications/basic science/technology - Bone healing

Wednesday, June 2 2010 / Room: N104
Time: 17:00 - 18:30

Moderator: David Finlayson (UK); Luis Meseguer (Spain)
Speaker: Kenji Tobita

Presentation	Pid	Title
not available	F91	Effect of low-intensity pulsed ultrasound stimulation on gap healing in a rabbit osteotomy model evaluated by quantitative micro computed tomography-based 3-dimensional cross-sectional moment and cross-sectional moment of inertia

Authors

Kenji Tobita, Isao Ohnishi, Takuya Matsumoto, Satoru Ohashi, Masahiko Bessho, Masako Kaneko, Juntaro Matsuyama, Kouzou Nakamura

Abstract

INTRODUCTION: Low-intensity pulsed ultrasound stimulation (LIPUS) reportedly enhances restoration of strength at fracture healing sites. However, evaluation of strength by mechanical testing was limited to only one direction, with either bending or torsion. Quantitative micro computed tomography (μCT) scans allow us to calculate strength-related parameters such as cross-sectional moment (CSM) and cross-sectional moment of inertia (CSMI). Previous studies have performed 2-dimensional (2D) analyses, and 3-dimensional (3D) evaluations have not been described. The purpose of this study was thus to investigate the effects of LIPUS on osteotomy healing using 3D analyses of CSM and CSMI. MATERIALS AND METHODS: Bilateral, transverse, mid-tibial osteotomies with a 2-mm gap were performed in 42 rabbits. LIPUS was continued for both the treatment group (n=7/group/time point) and the control group (n=7/group/time point), for 20 min, six times/week, for 4, 6, or 8 weeks. The control group also received a sham inactive transducer under the same condition as the LIPUS group. After the tibia was scanned by μCT, region of interest (ROI) was set at the center of the osteotomy gap with a width of 1 mm. Center of gravity for the ROI and the XYZ coordinate was calculated. An optional line (l) can be drawn in this coordinate. The angle of the Z axis (?) was measured, and also the degree of angle of the X axis (f) was measured. The 3D CSM [I (f, ?)] around this line was calculated using the following equation: I (f, ?) = ? r²dV (mm5), where r is the distance of a voxel to the center of gravity (mm) and dV is the area of a voxel (mm3). The axial CSM was defined as CSMx: I (0, 90), CSMy: I (90, 90), whereas the polar CSM was also defined as CSMp: I (any, 0). 3D CSMI weighted by density distribution was calculated using the following equation: I' (f, ?) = ? r²dm = ? ?r²dV (mg.mm²), ? is the measured volumetric callus mineral density. Likewise CSMIx, CSMIy and CSMIp were calculated. These data of the μCT evaluations were analyzed using a one-way ANOVA test ($p<0.05$). RESULTS: When 3D CSMs at the same time point were compared, values for the LIPUS groups were significantly higher than those for control groups for CSMx at 6 weeks and CSMp at 8 weeks. As for comparison of 3D CSMIs at the same time point, values for the LIPUS groups were significantly higher than those of the control groups for CSMIx, CSMIy, and CSMIp at 6 and 8 weeks. DISCUSSION: Bone healing by 3D CSM and CSMI has not been described before. Our results demonstrate that these bone strength parameters improved with LIPUS during the early phases. However, whether the late phase of callus formation is influenced remains unclear.

General Orthopaedic/ complications/ basic science/technology
Sports / knee soft-tissue
Hip
Knee osseous
Trauma / polytrauma
Spine (including trauma)
Shoulder/Elbow/ Arm/Forearm
Hand / wrist
Foot/Ankle/Leg
Paediatrics
Bone and Joint Tumour
Infection
Osteoporosis
Pain control / rehabilitation and non-surgical management
Trauma Upper Limb
Trauma Lower Limb

47º Congreso SECOT
Sociedad Española de Cirugía Ortopédica y Traumatología

11th Congress EFORT
European Federation of National Associations of Orthopaedics and Traumatology

MADRID, SPAIN 2 - 5 June 2010

Free Papers
E-Poster
Symposia
Instructional Lecture
Controversial Case Discussions
Guest Societies
ExMEx
Comprehensive Review Course
Satellite Symposia
Plenary Sessions
Comunicaciones SECOT
E-Poster SECOT
Sesiones SECOT
Index of Authors
Timetable
Search

E-Poster Content

CLOSE SESSION

Presentation	Pid	Title
not available	P285	Strength index by quantitative computed tomography-based finite element method offers higher discriminatory power for hip fracture than areal bone mineral density of the femoral neck

Authors

Isao Ohnishi, Masahiko Bessho, Takuya Matsumoto, Masako Kaneko, Satoru Ohashi, Kenji Tobita, Kozo Nakamura

Abstract

Introduction: We established a quantitative computed tomography (QCT)-based finite element (FE) method (QCT/FEM) that is able to more accurately quantify structural strength of the proximal femur compared to previous methods (Bessho et al., 2007). Previous experimental studies using mechanical testing of cadaver specimens disclosed that strength predicted by QCT/FEM correlated more closely with fracture load than the density value from dual energy X-ray absorptiometry (DXA) or QCT did (Cody et al., 1999). However, no previous studies have evaluated the discriminatory power of QCT/FEM for hip fracture. The aim of this study was thus to compare the discriminatory power of QCT/FEM to that of areal bone mineral density (aBMD) and volumetric bone mineral density (vBMD) by conducting a cross-sectional case-control study with osteoporotic women with and without hip fracture. Materials and Methods: Subjects comprised 41 women aged between 70 and 84 years old who completed a health examination in our institution from January 2008 to December 2008 (non-fracture group), and 30 patients aged between 70 and 84 years old with hip fracture (hip fracture group). The study protocol was approved by our ethics committee. Axial QCT was obtained for both the right proximal femur and a calibration phantom. From the QCT data, FE models were created (Bessho et al., 2007). Load and boundary conditions were applied to this model to represent two loading configurations, one approximating joint loading during single limb stance (stance configuration (SC)), and the other designed to simulate a fall on the greater trochanter (fall configuration (FC)). Materially nonlinear FE analysis was performed using the Newton-Raphson method (Bessho et al., 2007). Predicted fracture load was defined as proximal femoral strength index (PFSI). The same QCT scans were used to assess vBMD and aBMD of the proximal femur with commercially available software (QCT Pro), referring to the methods described by Bauer et al (2007). .A receiver operating characteristics (ROC) curve was drawn to calculate area under the curve (AUC) for PFSI, aBMD and vBMD. For each statistical analysis, differences were considered significant at $p<0.05$. Results: AUCs for PFSI in SC, PFSI in FC, aBMD and vBMD were 0.943, 0.957, 0.836, and 0.879, respectively. AUCs for PFSI in SC and FC were significantly larger than that for aBMD ($p<0.012$, $p<0.005$). Discussion: In the current investigation, strength index by QCT/FEM offered higher sensitivity and specificity for hip fracture discrimination than aBMD. The current study was basically a cross-sectional case-control study, but a prospective cohort study will be necessary in the future to investigate the discriminatory power of strength index by QCT/FEM for hip fracture.

General Orthopaedic/ complications/ basic science/technology
Sports / knee soft-tissue
Hip
Knee osseous
Trauma / polytrauma
Spine (including trauma)
Shoulder/Elbow/ Arm/Forearm
Hand / wrist
Foot/Ankle/Leg
Paediatrics
Bone and Joint Tumour
Infection
Osteoporosis
Pain control / rehabilitation and non-surgical management
Trauma Upper Limb
Trauma Lower Limb
Allied Professions

47º Congreso SECOT
Sociedad Española de Cirugía Ortopédica y Traumatología

11th Congress EFORT
European Federation of National Associations of Orthopaedics and Traumatology

MADRID, SPAIN 2 - 5 June 2010

Free Papers
E-Poster
Symposia
Instructional Lecture
Controversial Case Discussions
Guest Societies
ExMEx
Comprehensive Review Course
Satellite Symposia
Plenary Sessions
Comunicaciones SECOT
E-Poster SECOT
Sesiones SECOT
Index of Authors
Timetable
Search

E-Poster Content

CLOSE SESSION

Presentation	Pid	Title
not available	P180	Evaluation of the Accuracy of Articular Cartilage Thickness Measurement by Conventional and Real-time Spatial Compound Ultrasonography

Authors

Satoru Ohashi, Isao Ohnishi, Takuya Matsumoto, Masahiko Bessho, Kehji Tobita, Masako Kaneko, Juntaro Matsuyama, Kozo Nakamura

Abstract

The purpose of this study was to develop a method to objectively quantify articular cartilage thickness in vitro using both conventional and real-time spatial compound B-mode ultrasonography and to evaluate the accuracy of measurement. Knee joints were obtained for a 6-month- and a 3-year-old pig from a slaughterhouse. Osteochondral blocks with a surface size of 20 x 20 mm from the medial femoral condyle were acquired by cutting the bone with a band saw, and then fixed on a custom-made acryl sample holder (30 x 30 x 13 mm; Murai & Co., Tokyo, Japan) with resin. A B-mode 10.0-M Hz linear ultrasound probe (UST-5411; Aloka, Tokyo, Japan) connected to an ultrasound device (Prosound ALPHA 10; Aloka) was attached to a holding arm, which was fixed to a stage with an x, y micrometer for horizontal adjustment to enable identification of the location of cartilage measurement. B-mode images of the center line of the sample holder were acquired in the watertank. Image settings were for both conventional imaging and real-time spatial compound imaging superimposed with three frames each from a different viewing angle of - 20, 0, and 20 degrees to the right angle. Brightness line data of 32 points at 0.5-mm intervals in each image were obtained from both the 6-month- and 3-year-old pigs. The cartilage surface and cartilage-bone border of the specimen were defined as the peaks of each reflected signal. Cartilage thickness (Tc-US) was measured as the distance between peaks. Then, a center-cut plane of the acryl sample holder was created by the diamond saw device (Minitom; Struers, Westlake, OH), corresponding to the B-mode ultrasound image plane. Thickness of the cartilage (Tc) was measured at each point using optical measuring microscopy (MM-400; Nikon, Tokyo, Japan). Mean (± SD) values of Tc, Tc-US (conventional) and Tc-US (spatial compound) for both samples were 2.40 ± 0.39, 2.46 ± 0.42 and 2.40 ± 0.47 mm for a 6-month-old pig and 1.49 ± 0.10, 1.45 ± 0.18 and 1.47 ± 0.14 mm for a 3-year-old pig, respectively. Pearson's coefficients of correlation between Tc and Tc-US (conventional) and between Tc and Tc-US (spatial compound) were 0.892 and 0.947 for the 6-month-old pig and 0.696 and 0.753 for the 3-year-old pig, respectively. Tc-US from each setting was significantly correlated with Tc in both the 3-year- old and 6-month-old pigs ($p < 0.0001$ each). This is the first study to measure Tc using real-time spatial compound ultrasonography, which has been adopted in evaluating other tissues, such as tendon and ligament. From our results, real-time spatial compound ultrasonography may potentially have higher accuracy for measuring Tc than conventional methods, even though both showed good accuracy in our study. We believe the accuracy of our method is sufficiently high to allow application to measure human Tc in future studies.

General Orthopaedic/ complications/ basic science/technology
Sports / knee soft-tissue
Hip
Knee osseous
Trauma / polytrauma
Spine (including trauma)
Shoulder/Elbow/ Arm/Forearm
Hand / wrist
Foot/Ankle/Leg
Paediatrics
Bone and Joint Tumour
Infection
Osteoporosis
Pain control / rehabilitation and non-surgical management
Trauma Upper Limb
Trauma Lower Limb
Allied Professions

47º Congreso SECOT
Sociedad Española de Cirugía Ortopédica y Traumatología

11th Congress EFORT
European Federation of National Associations of Orthopaedics and Traumatology

MADRID, SPAIN 2 - 5 June 2010

Free Papers
E-Poster
Symposia
Instructional Lecture
Controversial Case Discussions
Guest Societies
ExMEx
Comprehensive Review Course
Satellite Symposia
Plenary Sessions
Comunicaciones SECOT
E-Poster SECOT
Sesiones SECOT
Index of Authors
Timetable
Search

Free Paper Content CLOSE SESSION

General Orthopaedic/complications/basic science/technology - Bone healing

Wednesday, June 2 2010 / Room: N104
Time: 17:00 - 18:30

Moderator: David Finlayson (UK); Luis Meseguer (Spain)
Speaker: Kenji Tobita

Presentation	Pid	Title
not available	F90	Effect of low-intensity pulsed ultrasound stimulation on callus remodeling in a gap healing model - Evaluation by bone morphometry using 3-dimensional quantitative micro computed tomography -

Authors

Kenji Tobita, Isao Ohnishi, Takuya Matsumoto, Satoru Ohashi, Masahiko Bessho, Masako Kaneko, Juntaro Matsuyama, Kouzou Nakamura

Abstract

INTRODUCTION: Low-intensity pulsed ultrasound stimulation (LIPUS) can enhance bone regeneration and callus healing during fracture repair. However, whether a certain phase of the healing process in fracture repair in particular is influenced by LIPUS treatment remains unclear. In this investigation, the effect of LIPUS on callus remodeling in a gap healing model was evaluated by bone morphometric analyses using 3-dimensional (3D) quantitative micro computed tomography (μCT) at the healing site, providing information on the temporal sequence of mineralized remodeling events that characterize the gap healing. MATERIALS AND METHODS: The rabbit osteotomy model with 2-mm gap for the right tibia was immobilized with four pins fixed to an external fixator with double side bars. LIPUS was continued for both the treatment group (n=7/group/time point) and the control group (n=7/group/time point), for 20 min, six times/week, for 4, 6, or 8 weeks. The control group also received a sham inactive transducer under exactly the same condition as the LIPUS group. After the harvested tibia was scanned by μCT, region of interest was set at the callus healing area. It defined as a center of the osteotomy gap with a width of 1 mm. Morphometric parameters used for evaluation were mineralized callus volume (BV, cm^3) and volumetric bone mineral density of mineralized tissue comprising the callus (mBMD, mBMD = BMC/BV, $mgHA/cm^3$). The whole ROI was measured and was subdivided into three zones. The periosteal callus zone (External) , the medullary callus zone (Endosteal) and the remaining zone was the cortical gap zone (Intercortical). For each zone, BV and mBMD were measured. Data of the μCT evaluations were analyzed using a one-way ANOVA test. Statistically significant difference was set at $p < 0.05$. RESULTS: In the LIPUS groups, BV for the Endosteal zone was significantly lower for the 8-week group than for the 4-week group. Comparing results at the same time point, the LIPUS group at 8 weeks was significantly higher than that of the control group in the Intercortical zone. As for mBMD, in the LIPUS group, the 8-week group was significantly higher than the 4-week group for Total, External, Internal, and Endosteal zones, respectively. Comparing results at the same time point, mBMD was significantly higher for the LIPUS group at 8 weeks than for the control group in both External and Intercortical zones. DISCUSSION: The most striking finding in our study was that LIPUS accelerated bone formation in the Intercortical zone and callus resorption in the Endosteal zone. This suggests that LIPUS could shorten the time required for remodeling. However, the results of this study do not clarify whether an early phase in callus formation in particular is influenced by LIPUS.

General Orthopaedic/ complications/ basic science/technology
Sports / knee soft-tissue
Hip
Knee osseous
Trauma / polytrauma
Spine (including trauma)
Shoulder/Elbow/ Arm/Forearm
Hand / wrist
Foot/Ankle/Leg
Paediatrics
Bone and Joint Tumour
Infection
Osteoporosis
Pain control / rehabilitation and non-surgical management
Trauma Upper Limb
Trauma Lower Limb

47º Congreso SECOT
Sociedad Española de Cirugía Ortopédica y Traumatología

11th Congress EFORT
European Federation of National Associations of Orthopaedics and Traumatology

MADRID, SPAIN 2 - 5 June 2010

Free Papers
E-Poster
Symposia
Instructional Lecture
Controversial Case Discussions
Guest Societies
ExMEx
Comprehensive Review Course
Satellite Symposia
Plenary Sessions
Comunicaciones SECOT
E-Poster SECOT
Sesiones SECOT
Index of Authors
Timetable
Search

Free Paper Content CLOSE SESSION

Lower limb - Lower extremities (3 Minutes Free Paper)

Friday, June 4 2010 / Room: Neptuno
Time: 08:30 - 10:30

Moderator: Thierry Bégué (France); Pedro Carpintero (Spain)
Speaker: Masako Kaneko

Presentation	Pid	Title
not available	F446	Prediction of proximal femur strength by a quantitative computed tomography-based finite element method -Creation of predicted strength data of the proximal femur according to age range in a normal population and analysis of risk factors for hip fracture-

Authors

Masako Kaneko, Isao Ohnishi, Masahiko Bessho, Takuya Matsumoto, Satoru Ohashi, Kenji Tobita, Kozo Nakamura

Abstract

Introduction: There is a clear need for the development of more sensitive risk assessment tools for clinical predictors of fractures. Bone densitometries are limited in the ability to account for complex geometry, architecture, and heterogeneity of bone. Quantitative computed tomography (QCT)-based finite element (FE) methods (QCT/FEM) are able to perform structural analyses taking these factors into consideration to accurately predict bone strength. However, no basic data have been available regarding predicted strength (PS) of the proximal femur by QCT/FEM with reference to age in a normal population. The purpose of this study was thus to create a database on PS in a normal population as a preliminary trial. With these data, parameters that affect PS were also analyzed. Methods: Participants in this study comprised individuals who participated in a health checkup program with computed tomography (CT) at our hospital in 2008. Participants included 487 men and 237 women (age range, 40-87 years). Exclusion criteria were provided. Scan data of the proximal femur were isolated and taken from overall data from CT of each participant with simultaneous scans of a calibration phantom containing hydroxyapatite rods. A FE model was constructed from the isolated data using Mechanical Finder software. For each of the FE models, loading and boundary conditions as well as the definition of PS were exactly the same as described by Bessho et al. (Bone 2009). For each participant, height, weight, and abdominal circumference (AC) were measured. The analyses included linear regression analysis relating age and PS, one-way analysis of variance to compare average PS among the groups of participants who were divided into 5-year age brackets, and multiple regression analysis to determine how PS was affected by age, height, weight, and AC. Differences were considered significant for values of $p<0.05$. Result: The following results were obtained. First, average PS was lower in women than in men for all age ranges. Second, PS in men under stance configuration, and those in women under stance and fall configurations significantly decreased with age. Third, weight positively affected PS in both men and women. Discussion: This was the first study to investigate changes in PS with age in a normal population. Whether PS by QCT/FEM correlates more closely with fracture risk for osteoporotic patients in comparison to other bone densitometries remains unclear, but the our results did not contradict any existing concept of risk factors for fragility fracture. More baseline data for PS in normal populations need to be accumulated by increasing the number of participants in studies like this.

General Orthopaedic/ complications/ basic science/technology
Sports / knee soft-tissue
Hip
Knee osseous
Trauma / polytrauma
Spine (including trauma)
Shoulder/Elbow/ Arm/Forearm
Hand / wrist
Foot/Ankle/Leg
Paediatrics
Bone and Joint Tumour
Infection
Osteoporosis
Pain control / rehabilitation and non-surgical management
Trauma Upper Limb
Trauma Lower Limb

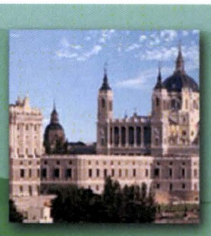

47º Congreso SECOT
Sociedad Española de Cirugía Ortopédica y Traumatología

11th Congress EFORT
European Federation of National Associations of Orthopaedics and Traumatology

MADRID, SPAIN 2 - 5 June 2010

Free Papers
E-Poster
Symposia
Instructional Lecture
Controversial Case Discussions
Guest Societies
ExMEx
Comprehensive Review Course
Satellite Symposia
Plenary Sessions
Comunicaciones SECOT
E-Poster SECOT
Sesiones SECOT
Index of Authors
Timetable

Search

E-Poster Content

CLOSE SESSION

Presentation	Pid	Title
not available	P157	Analysis of lag screw bone interface mechanics using a patient-specific finite element method

Authors

Takuya Matsumoto, Isao Ohnishi, Bessho Masahiko, Satoru Ohashi, Kenji Tobita, Masako Kaneko, Kozo Nakamura

Abstract

The risk of cut out by the screw is one of the most serious problems of osteosynthesis for osteoporotic hip fracture. The aim of this study was to assess stress and strain at a lag screw and bone interface using computer-aided design (CAD) data for a lag screw and patient-specific 3-dimensional (3D) finite element (FE) analysis (FEA). And the risk was predicted using the results of this FEA, and optimization of screw placement was performed. FE model with and without osteoporosis, for an osteoporotic model, femur of a female patient aged 83 with contra-lateral trochanteric fracture, and for a non-osteoporotic one, femur of a female patient aged 30 with contra-lateral osteomyelitis of the femur were created and analyzed. Computed tomography of the femur and a calibration phantom were obtained. CAD data for a compression hip screw system were supplied by the manufacturer (Mizuho Co Ltd., Japan). Data were transferred to a computer, and 3D FE models of the proximal femur with lag screw and angle plate in place were constructed using Mechanical Finder. The screw was inserted at the center of the femoral neck in the sagittal plane parallel to the axis. In the coronal plane, 4 different screw positions were created; just above the calcar femorale (CF); 5 mm, 10 mm, 15 mm proximal to CF individually. The outer surface of the cortical bone was modeled with 3 nodal-point shell elements with a thickness of 0.4 mm and a variable side length of 1.0-4.0 mm. The rest of the bone and implants were modeled using tetrahedral elements with a variable side length of 1.0-4.0 mm. Mechanical properties of bone and shell elements were heterogeneous, the same as reported by Bessho et al. (2007). Mechanical properties of elements constructing implants were the same as 6-aluminum 4-vanadium titanium alloy. Bone/implant interface was bonded completely, while gap elements were applied at the lag screw/angle plate interface. Loading and boundary conditions represent stance configuration with a compressive load of 980 N. Linear FEA was conducted for each model, and the minimum principal strain and equivalent stress were calculated for each of the screw height conditions. Analysis of minimum principal strain and equivalent stress showed that the high value area tended to widen in a patient with osteoporosis, and that the more proximally the screw was inserted, the area with high equivalent stress widened at CF. Therefore, in severely osteoporotic patients, placement of screws must be carefully planned to avoid postoperative cut out after fixation. The FE method utilized in this study would be useful for preoperative planning and management in assisting to determine how much weight-bearing should be allowed postoperatively.

General Orthopaedic/ complications/ basic science/technology
Sports / knee soft-tissue
Hip
Knee osseous
Trauma / polytrauma
Spine (including trauma)
Shoulder/Elbow/ Arm/Forearm
Hand / wrist
Foot/Ankle/Leg
Paediatrics
Bone and Joint Tumour
Infection
Osteoporosis
Pain control / rehabilitation and non-surgical management
Trauma Upper Limb
Trauma Lower Limb
Allied Professions

2010 IEEE International Conference on Robotics and Automation
Anchorage Convention District
May 3-8, 2010, Anchorage, Alaska, USA

Hazard Analysis of Fracture-Reduction Robot and its Application to Safety Design of Fracture-Reduction Assisting Robotic System

Sanghyun Joung[1], Hongen Liao[1], Etsuko Kobayashi[1],
Mamoru Mitsuishi[1], Yoshikazu Nakajima[1], Nobuhiko Sugano[2], Masahiko Bessho[3],
Satoru Ohashi[3], Takuya Matsumoto[3], Isao Ohnishi[3], and Ichiro Sakuma[1]

Abstract— **In this paper, we discuss the issue of safety in robot-assisted fracture reduction. We define the hazards of robot-assisted fracture reduction and design safety control methods. Although a large reduction force is required to reduce femoral neck fractures, an unexpectedly large force produced by a robot may cause injury to the patient. We have designed two mechanical failsafe units and a software force limiter; this along with velocity control can guarantee a safe operation in reduction force. In addition, to reduce the movement of bone fragments as much as possible, we devised spatially constrained control methods for fracture-reduction robots. The fracture-reduction system was evaluated using simulated fracture reductions.**

I. INTRODUCTION

Hip fractures occur at the proximal end of the femur. The cause of most hip fractures is low-energy trauma, which is associated with falling from a standing height or lower, in elderly patients with osteoporosis. Using the epidemiologic literature on hip fracture incidence in various regions of the world and demographic projections, Cooper et al. estimated that the number of hip fractures occurring globally each year will rise from 1.66 million in 1990 to 6.26 million by 2050 [1].

Most patients with hip fractures undergo surgery. An operation comprises two processes: reduction and fixation of bone fragments. The fracture must be reduced before fixing the bone fragments, and pulling of bone fragment in this procedure requires a large reduction force. Conventional fracture reduction is often achieved using a fracture table. However, fracture tables have less degrees of freedom (DOF), which is one of the reasons why reduction is often inadequate. This may cause complications such as nonunion of the fracture [2]. Further, there are no safe methods available for avoiding the application of excessive force to the injured limb, which can lead to damage of the soft tissue around the bone fragment. Moreover, repeated exposure to radiation sustained by surgeons and medical staff is a well-known problem in the field of orthopedic surgery [3].

Füchtmeier et al. [4] introduced RepoRobo, a robotic system for assisting fracture reduction. They converted a commercial industrial robot for medical use by appropriate modifications. The requirements for using an industrial robot for reduction of femoral shaft fractures *in vitro* are well described. They did not, however, provide any experimental results. Westphal et al. [5] and references therein also tried to use an industrial robot for medical use. They tried to develop a surgical telemanipulator system to support long-bone fracture reduction procedures.

Studies prior to the work described in this paper were conducted by Mitsuishi et al. [6]. In Mitsuishi's system, the foot is fixed using a fracture boot, as in conventional fracture reduction methods. The authors have already reported navigation-based control of the system [7]. Another application of the proposed system is power assistance, where the robot augments the surgeon's force to generate the power required for fracture reduction. The reduction path and reduction force/torque also need to be controlled so that bone fracture reduction is conducted safely. In this study, we analyzed the hazards of robot-assisted fracture reduction in power assistance mode and designed countermeasures for hazard prevention. We then carried out an experimental evaluation of the proposed system for robot-assisted fracture reduction.

II. SAFETY AND SYSTEM DESIGN

In the case of an industrial robot, the major strategy for ensuring human safety is to physically separate the robot from vulnerable humans by creating a safe robot workspace from which humans are excluded. However, this strategy is obviously inappropriate in the case of a surgical robot, where the application demands interaction between the robot and humans in the same workspace and even direct operation on human subjects. Surgical robots must therefore have safety features that are appropriate to such applications in addition to the safety features currently required for industrial robot application.

A. Hazards of fracture reduction

Fig. 1 shows the hazards related to robot-assisted fracture reduction. The conventional method for fracture reduction is indirect reduction. A direct reduction method, which requires the insertion of external devices to fix the bone fragment, was devised to improve reduction accuracy, and a robotic system was introduced to assist surgeons in reducing fractures more accurately and steadily. Though the accuracy of the reduction can be increased by application of the new technique to the conventional method, the extended system also results

[1]Graduate School of Engineering, the University of Tokyo, 7-3-1 Bunkyo-ku, Tokyo, Japan, shjoung@bmpe.t.u-tokyo.ac.jp
[2]Graduate School of Medicine, Osaka University, Japan,
[3]Graduate School of Medicine, the University of Tokyo Hospital, Japan

978-1-4244-5040-4/10/$26.00 ©2010 IEEE

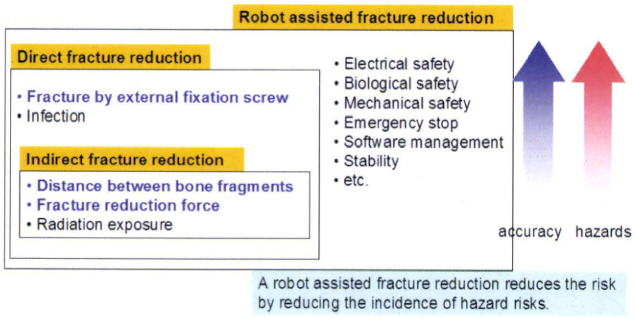

Fig. 1. List of hazards associated with robot-assisted fracture reduction

in an increase in the number of hazards. However, if the robotic system is able to control the hazards satisfactorily, the application of this system could increase reduction accuracy with lower risk. This paper presents an analysis of hazards in a robot-assisted fracture-reduction system for use in direct reduction methods, details of the implementation of safety countermeasures, and evaluation of results.

1) Distance between the bone fragments: Excessive traction may injure the sciatic nerve, which starts in the lower back and runs through the buttock and down the lower limb and serves nearly the whole of the skin of the leg, the muscles of the back of the thigh, and those of the leg and foot. Though traction motion of the limbs is required, it must be within a safe range. The safe range of traction distances recommended by surgeons is $25mm$ to $30mm$ between the proximal and distal bone fragments. A navigation system can measure the distance between the two bone fragments. A safe range can be kept by stopping the robot when the navigation system sounds an alarm for over-traction of the distal bone fragments. We have developed control software to provide constraints on robot motion to avoid excessive displacement of bone fragments.

2) Fracture-reduction force: Excessive reduction force may cause injury to the soft tissues of the limbs. Therefore, fracture-reduction robots need to have some functions that can limit the reduction force to a safe range. A fracture-reduction robot, named FRAC-robo, which is the predecessor of the fracture-reduction robot in this study, was used to monitor the traction force and the rotation torque in the reduction of proximal femoral fractures [9]. The average maximum traction force and rotation torque are $215.9N$ and $3.2Nm$, respectively. Although some clinical data have been reported, the safe range for fracture-reduction forces has not been clear up until now. A force limiter for controlling the fracture-reduction force has therefore been designed so that the force limit can be adjusted.

B. System design

We addressed the following two requirements when designing a robot to conduct fracture reduction with high levels of safety and accuracy:

- restriction of displacement of bone fragments to allowed values to prevent damage to soft tissues surrounding the bone and
- restriction of the applied force/torque on the bone fragment to avoid damage to the bone fragment.

In order to satisfy these requirements, we developed safety modules and a robot control method. The hardware layer of the robot has two mechanical failsafe units and a force sensor; the two mechanical failsafe units limit the reduction force, which is one of the system's hardware performance features. Data from force sensors are used to measure reduction force. The gain of the system speed controller was automatically adjusted to reduce the velocity of the fracture-reduction robot. Ensuring that there is little movement of the bone fragment can reduce the displacement of soft tissues around the bone fragment, thus, this reducing the risk of soft-tissue damage. A spatial constraint power assistance mode that constrains the rotation center at a point on the fracture surface of the bone fragment was developed to make highly accurate small movements of the bone fragment. The actual safety designs for these will be described in the next chapter.

III. Fracture-Reduction Assisting System

An example of the configuration of a fracture-reduction system is shown in Fig. 2. The fracture-reduction system consists of a fracture-reduction robot and a navigation system. The surgical bed and the fracture-reduction robot are arranged in a line. One side of the surgical bed is used for the navigation system, and the other side is used by the surgeon who reduces the fracture and fixes the bone fragments.

A. Fracture-reduction robot

The structure of the fracture-reduction robot is shown in Fig. 3(a); a kinematic model and the robot coordinates are provided in Fig. 3(b).

The fracture-reduction robot has six DOFs (i.e., three translation DOFs and three rotation DOFs). Three rotational axes intersect each other at one point, to give robot controls which are easily calculated kinematically. Translation along the y-axis and rotation around the y-axis has a mechanical failsafe unit which can mitigate excessive force. We installed a customized jig to fix the bone fragment to the robot. A

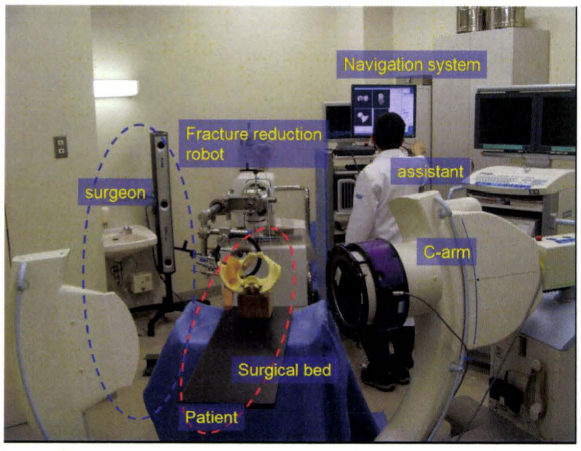

Fig. 2. Fracture-reduction system configuration

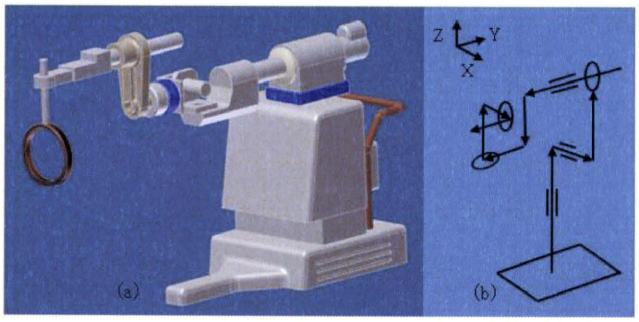

Fig. 3. Fracture-reduction robot; (a) outline, two blue parts show mechanical failsafe units and (b) kinematic model and coordinates of the robot

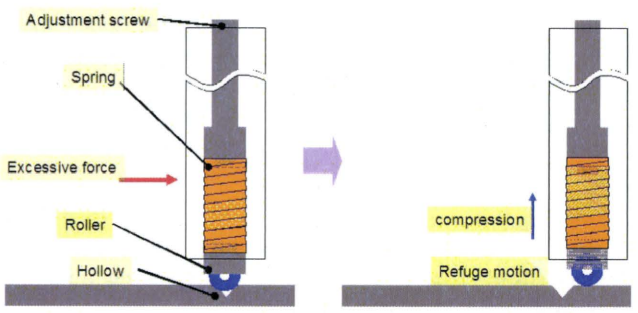

Fig. 4. Structure of translational failsafe mechanism

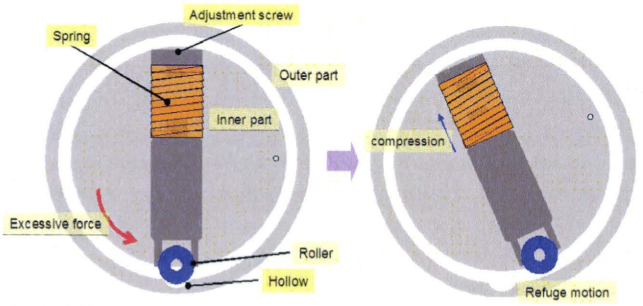

Fig. 5. Structure of rotational failsafe mechanism

force-moment sensor (IFS-105M50A220-I63; Nitta, Osaka, Japan) is mounted on an end effector of the machine unit in order to monitor fracture-reduction forces and torques. The user interface is a touch panel. We installed four emergency buttons; all movements of the robot stop if a button is pressed. A four-color LED array bar shows the robot status: Power On, Ready, Operating, and Emergency Stop. Four steerable wheels attached beneath the robot enable medical staff to move the robot easily, in spite of its weight ($315kg$). The dimensions of the robot are 640 mm (width) $\times$ 1,084 mm (length) $\times$ 1,317 mm (height). This size makes it possible to transport the robot in a normal passenger elevator.

B. Mechanical failsafe unit

Excessive reduction force may injure soft tissues of the limbs. The fracture-reduction robot must therefore have mechanical units that can limit the reduction force to a safe range. The robot has two mechanical failsafe units, which can mitigate excessive reduction forces. The installed positions of them are illustrated with blue parts in Fig. 3(a). These units maintain high rigidity within the allowed force and torque ranges. However, if an excessive force is applied to the unit, it decouples the end effector of robot from the actuation unit to remove the applied force or torque and prevent excessive force, which might damage the soft tissues, on the bone fragment. The longitudinal direction of the bone fragment coincides approximately with the traction direction of the robot. Surgeons should ensure that these positional relations are correct as the first step in surgery. If these positional relations are ensured, the traction failsafe unit can limit the traction force of the bone fragment, and the rotation failsafe unit is in operation while internal or external rotation of the bone fragment is conducted. Though Warisawa et al. [8] had reported the mechanical failsafe for an indirect fracture redution, we modified the units for a direct fracture reduction and described more details about these units.

The traction failsafe unit is installed on the y-axis of the fracture-reduction robot; this unit has a plunger with a steel roller pushed into a hollow by a spring (Fig. 4). The threshold force can be adjusted from $200N$ to $400N$ by adjustment of the screw, which can change the spring compression force.

The rotational failsafe unit is mounted between the customized jig and the tip of the robot. The mechanism is similar to that of the traction failsafe unit, as shown in Fig. 5. The threshold is adjustable from $20Nm$ to $40Nm$ by controlling the length of the spring. When the unit is decoupled, the rotation range of the customized jig is constrained by mechanical stoppers, the positions of which can be varied from $30°$ to $120°$.

A threshold can be calculated by considering the equilibrium of force and moment with two parameters, the spring force and the contact angle between a roller and a hollow. Fig. 6 shows the forces acting on the roller. F_s is the spring force. F_{ex} is the external force. N is the vertical component of force acting on a contact point between the roller and the hollow and is equal to F_s. W denotes the horizontal component of force acting on the contact point and is equal to F_{ex}. The following equation can be found by considering the moment equilibrium at the center of the roller

$$F_s r \sin\theta = F_{ex} r \cos\theta \tag{1}$$

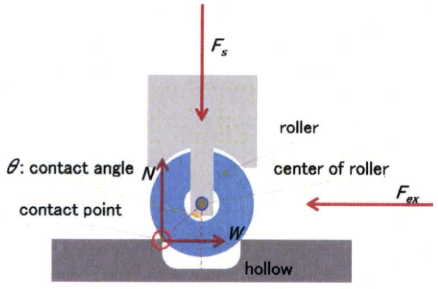

Fig. 6. Forces acting on roller and hollow

Here r is the radius of the roller and θ is the contact angle. From (1), the spring force for constraining the given F_{ex} can obtained by

$$F_s = kx = \frac{F_{ex}}{\tan\theta} \tag{2}$$

Here, k denotes the spring constant and x is the displacement of spring. A similar idea can be applied to the rotational failsafe unit, which gives

$$F_s = \frac{F_{ex}}{R\tan\theta} \tag{3}$$

Where, R is the radius of the inner part of rotational failsafe unit. Specifications for the mechanical failsafe units are shown in Table I. From (2) and Table 1, $2.5mm$ displacement of the spring made by the adjust screw is needed to set the threshold to $200N$ and $4.9mm$ displacement is required for $400N$ with the translational failsafe unit. We selected an adjust screw with the pitch of $3.0mm$. It is larger than the difference between above two displacements, so that we can adjust thresholds within single rotation of the adjustment screw. A similar idea was applied to the rotational failsafe unit.

TABLE I
SPECIFICATION FOR THE MECHANICAL FAILSAFE UNITS

		translation	rotation
Threshold range, N or Nm		200-400	20-40
radius of roller, mm		9.5	8
contact angle, °		34	45
spring	constant, N/m	121	204
	allowable displacement, mm	14.7	6.8
adjustment screw (pitch, mm)		M27 (3.0)	M22 (2.5)
radius of inner part, mm			50

The performances of the two failsafe units were evaluated. The end effector of robot was pulled out or was rotated by a human until the failsafe unit was activated, and the maximum force was recorded using the force sensor. Traction direction thresholds were set at $\pm 200N$, $\pm 300N$, and $\pm 400N$ at each evaluation. The rotational direction thresholds were set at $\pm 200Ncm$, $\pm 300Ncm$, and $\pm 400Ncm$. Five tests were conducted at each threshold. Fig. 7 shows the evaluation results. The variation in each of the five trials is shown by a bar. In the case of the traction direction, it was found that the test values were significantly smaller than the set values; the set value is the value at which the threshold is set, and the test value is the experimental result for the set value. This difference results from the weakened offset tension of the spring, which occurs when the robot is reassembled for correction of movement. The difference may be reduced by adjusting the offset tension. Long-term performance should be evaluated considering the variation of the offset tension and the durability of the mechanical structure.

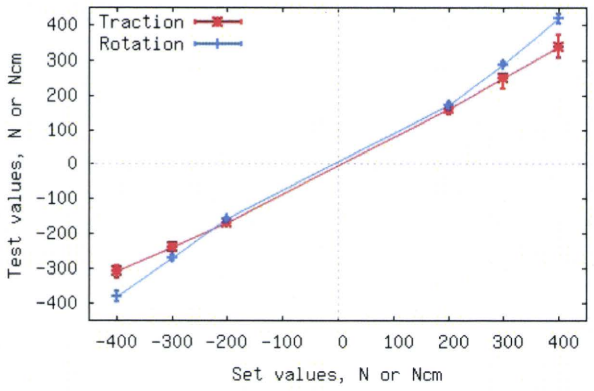

Fig. 7. Performance of failsafe mechanism, n=5

C. Software force limiter

The software force limiter is also designed to prevent excessive reduction force. The velocity gain is controlled against the measured force, as shown in (4).

$$G(t) = \begin{cases} 1 & F(t) < Th1 \\ \frac{(F(t)-Th1)^2}{(Th2-Th1)^2} & Th1 \leqq F(t) < Th2 \\ 0 & F(t) \geqq Th2 \end{cases} \tag{4}$$

Here, $F(t)$ is the measured fracture-reduction force, $Th1$ and $Th2$ are the first and second thresholds of the software limiter, and $G(t)$ is the velocity gain. Two thresholds are used, not only to avoid sudden stopping of the robot, but also to forewarn the operator of an increase in the reduction force by decelerating the robot. The robot speed is calculated using (5) and is slowed down according to a quadratic curve between the two thresholds.

$$V(t) = \alpha G(t) F(t) \tag{5}$$

Here α is a weighting factor and $V(t)$ is the control velocity of the robot. We set two thresholds of the software force limiter below the limiting force of the mechanical failsafe mechanism so that excessive force can be mitigated by the software force limiter. However, the mechanical failsafe mechanism is only operated when software problems occur.

The software force limiter was evaluated using a static obstacle. The robot moved in the direction of the x-axis, and the robot's velocity was set at $10mm/s$. A static obstacle was placed beside the customized jig to increase the reaction force. Two thresholds were set at $100N$ and $150N$, respectively. The robot's position was recorded with the robot's rotary encoder, and the reaction forces were measured using a built-in force sensor with a frequency of $50Hz$.

Fig. 8 shows the variations in the measured force and in the velocity. The jig contacted the obstacle within $5s$, and the force increased slowly. The force approached the first threshold at about $7s$, and the speed of the robot slowed down with the designed gain. The robot was stopped as

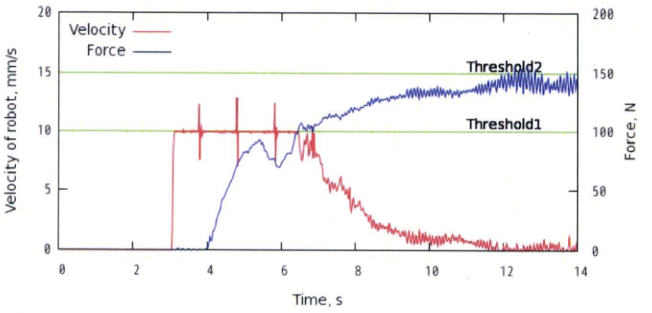

Fig. 8. Evaluation results for the software force limiter

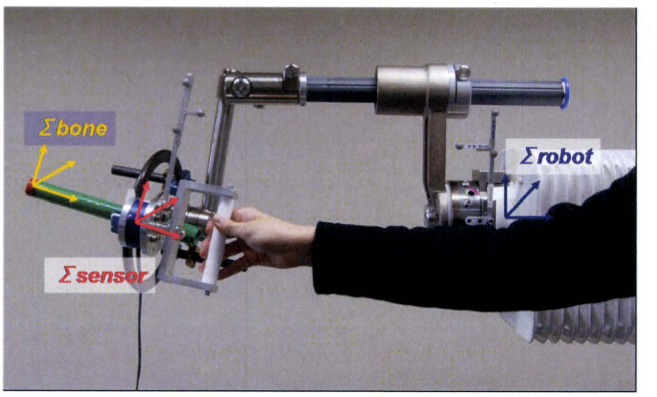

Fig. 9. Configuration of direct fracture reduction using fracture-reduction robot

the force reached the second threshold. Some spikes can be found in the velocity variation. The rotary encoder signals were recorded as a user-level task (non-real-time process) so as not to interrupt the main process. Thus the measurement frequency of $50Hz$ was not guaranteed. This is considered to be one cause of the spikes. This should be reconfirmed using a real-time measurement system. The usefulness of the software force limiter will be evaluated from a simulated fracture reduction with manual operation of the robot.

D. Control method for safe power assistance by the robot

In common hip fracture cases, the distal bone fragment is pulled up to the upper body and rotated externally by the influence of soft tissues. The surgeon therefore draws the distal bone fragment and then rotates it internally to reduce the fracture. The fracture-reduction robot reduces the fracture by a similar process, and provides an intuitive control method: a spatially constrained power assistance mode. Compared with indirect reduction methods, direct methods provide a larger number of DOFs for manipulating the bone fragments. However, direct methods also generate additional risks of damage to soft tissues and bone fragments (in particular at the bone/insertion pin interface).

To achieve safe direct fracture reduction, constraints on the bone fragment trajectory should be properly applied by surgeons to bone fragment manipulation.

We therefore introduced the following control method. In the proposed control method, the fracture-reduction robot can move each axis of the robot center on the bone coordinates. The origin of the bone coordinates is at the center of the fracture surface, and its primary axis is aligned with the longitudinal direction of the bone fragment. Surgeons can track the bone fragment along its longitudinal direction or can rotate the bone fragment centering on one point; these movements are safer and more intuitive than movement centered on the robot's coordinates. We abbreviated this control mode 'RCC-PA'(Rotation Center Constrained Power Assistant). The algorithm is as follows. The method supposes that the force and moment applied to the bone fragment by the surgeon are in his intended direction of movement, and that the magnitude of the force or moment is proportional to the velocity of the bone movement. The play of each axis is then calculated by considering the bone fragment and the robot as a rigid body. The problems to be solved are how to measure the force given to the bone fragment and how to measure and decide the bone's coordinates.

An additional force sensor (IFS-67M25A50-I40; Nitta, Osaka, Japan) was installed to measure the force given to the bone fragment, as shown in Fig. 9. The sensor was positioned between the handle and the ring-type frame holding the external fixation screws. The surgeon controls the bone fragment using the handle. The navigation system will be used to determine the bone's coordinates [10]. The navigation system measures and integrates the coordinates of the robot, the force sensor, and the fluoroscope, and calculates the coordinates using 2D-3D registration. The fracture-reduction robot receives the coordinate information from the navigation system. The force given to the bone fragment can be calculated using (6).

$$\begin{bmatrix} {}^{B}\mathbf{f} \\ {}^{B}\mathbf{m} \end{bmatrix} = \begin{bmatrix} {}^{B}\mathbf{R}_S & \mathbf{0} \\ [{}^{B}\mathbf{P}_S\otimes]\,{}^{B}\mathbf{R}_S & {}^{B}\mathbf{R}_S \end{bmatrix} \begin{bmatrix} {}^{S}\mathbf{f} \\ {}^{S}\mathbf{m} \end{bmatrix} \tag{6}$$

Here,

$$if\ \mathbf{a} = \begin{bmatrix} a_x \\ a_y \\ a_z \end{bmatrix},\ [\mathbf{a}\otimes] = \begin{bmatrix} 0 & -a_z & a_y \\ a_z & 0 & -a_x \\ -a_y & a_x & 0 \end{bmatrix} \tag{7}$$

${}^{\mathbf{A}}\mathbf{f}$(or ${}^{\mathbf{A}}\mathbf{m}$) is the force(or moment) at the given coordinates of "A". And ${}^{\mathbf{A}}\mathbf{R}_{\mathbf{B}}$ and ${}^{\mathbf{A}}\mathbf{P}_{\mathbf{B}}$ are the rotation matrix and the translation matrix, respectively. "S" denotes sensor coordinates and "B" denotes bone coordinates. And we used subscripts of "o", "p", and "g" to abbreviate the expressions of "original position", "present position", and "goal position", respectively.

Then, ${}^{B_p}\mathbf{T}_{B_g}$, a translation matrix from the present bone coordinate to the surgeon's target bone coordinate, is calculated from ${}^{\mathbf{B}}\mathbf{f}$ and ${}^{\mathbf{B}}\mathbf{m}$ using (8).

$$
\begin{aligned}
{}^{B_p}\mathbf{T}_{B_g} &= \begin{bmatrix} {}^{B_p}\mathbf{R}_{B_g} & {}^{B_p}\mathbf{P}_{B_g} \\ \mathbf{0} & 1 \end{bmatrix} \qquad (8)\\
{}^{B_p}\mathbf{R}_{B_g} &= \begin{bmatrix} k_x k_x vt + ct & k_x k_y vt - k_x st & k_x k_z vt + k_y st \\ k_x k_y vt + k_x st & k_y k_y vt + ct & k_y k_z vt - k_x st \\ k_x k_z vt - k_y st & k_y k_z vt + k_x st & k_z k_z vt + ct \end{bmatrix} \\
{}^{B_p}\mathbf{P}_{B_g} &= {}^{B}\mathbf{f}
\end{aligned}
$$

Here st, ct and vt denote $\sin(t)$, $\cos(t)$ and $1-\cos(t)$, respectively. $\mathbf{R}$ is the rotation of t° around the rotation axis, $\mathbf{K}$, which is given by (9). The t is proportional to $|{}^{B}\mathbf{m}|$.

$$
\mathbf{K} = \begin{bmatrix} k_x \\ k_y \\ k_z \end{bmatrix} = \frac{1}{|{}^{B}\mathbf{m}|}\,{}^{B}\mathbf{m} \qquad (9)
$$

${}^{B_p}\mathbf{R}_{B_g}$ or ${}^{B_p}\mathbf{P}_{B_g}$ is set as $\mathbf{I}$ or $\mathbf{0}$ in order to separate translational movement and rotational movement during fracture reduction.

The ${}^{R_p}\mathbf{T}_{R_g}$, which describes translation from the present robot position to the goal position, can be calculated from the given coordinates and ${}^{B_p}\mathbf{T}_{B_g}$ using (10).

$$
{}^{R_o}\mathbf{T}_{R_g} = {}^{R_o}\mathbf{T}_{R_p}\,{}^{R_p}\mathbf{T}_{B_p}\,{}^{B_p}\mathbf{T}_{B_g}\,{}^{B_g}\mathbf{T}_{R_g} \qquad (10)
$$

${}^{B_g}\mathbf{T}_{R_g}$ is the inverse matrix of the ${}^{R_p}\mathbf{T}_{B_p}$, because the positional correlation between the bone and the robot is not changed when the robot is moved.

${}^{R_o}\mathbf{T}_{R_g}$ can be expressed as six parameters, i.e., three translations and three rotations, and the present position of the robot is calculated by reading the six rotary encoders of the axis. Then, the difference between the present position and the goal position gives the distance moved for each axis.

The accuracy of the RCC-PA method was evaluated. The bone, sensor, and robot coordinates were set using an optical 3D position measurement system (Polaris; NDI, Waterloo, Ontario, Canada). The origin position of the bone coordinate was measured in the robot coordinate as the RCC-PA was being conducted. The ideal movement is zero. We therefore treat the distance moved by the origin of the bone coordinate from the initial position as the control error. The movement of the axis influences the control error because the fracture-reduction robot is a serial construct. Each movement of the axis is also measured to estimate these effects.

Fig. 10 shows the control error and the play of each axis. The control error is within $2mm$ and is less than the play of the axis. Both quantities are larger at the x- and z-axes, which are related to the rotation axis.

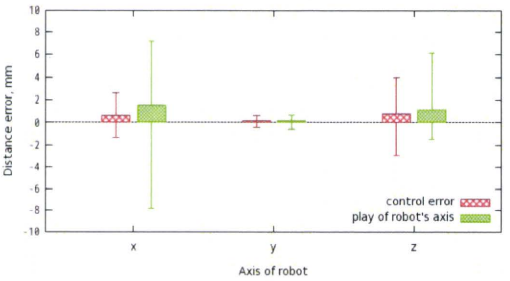

Fig. 10. RCC-PA motion distance error

IV. Experiments

The developed fracture-reduction system was evaluated by simulated fracture reduction using hip fracture models. The hip fracture model was prepared by cutting a femur model (Composite Femur; Pacific Research Laboratories, Inc., Vashon, WA, USA) with a band saw, and attaching a rubber band between the femur and the hip to simulate the influence of muscles such as the gluteus medius and the piriformis.

A fracture reduction is generally assessed using 2D fluoroscopic images. The reduction alignment angles of the anteroposterior (AP) and lateral views should be within the defined values; however, this assessment is influenced by the measured angle of the fluoroscopic images, as well as by the surgeon's viewpoint. Therefore, to ensure high reproducibility, we evaluated the reduction results from parameters related to the mechanical axis used to assess the femur deformity [11]. The mechanical axis is drawn from the center of the knee joint to the head of the femur. If the mechanical axis is defined, the mechanical distal femur angle (DFA) and the proximal femur angle (PFA) can also be defined. DFA is the angle between the mechanical axis and a tangent through the two most convex distal points of the femoral condyles, and PFA is the angle between the mechanical axis and a line from the tip of the greater trochanter to the hip center. Before fracturing the femur model, we marked feature points such as the greater trochanter, the head of the femur, the lateral condyle, and the medical condyle. We measured the 3D positions of the feature points using a pen-type reference marker and the optical 3D position measurement system. We then calculated the normal values of the length of the mechanical axis, the PFA, and the DFA from the four measured feature points. The reduction values after the fracture reduction were compared to the normal values.

A. Experimental setup

The fracture model was positioned on the surgical bed. The customized jig for connecting the bone fragment to the robot was positioned near the fracture model using a jog operation and the distal bone fragment of the fracture model was connected to the jig.

Fracture reduction using the RCC-PA mode was conducted eight times in open conditions, which means that the fracture site could be seen directly. The fracture-reduction procedure was divided into three steps as follows. First, longitudinal traction of the distal bone fragment was performed. Second, the posture of the distal bone fragment was modified. The main movement was internal rotation of the bone fragment while the center of rotation was constrained. Finally, the distal bone fragment was repositioned, and fine control of the alignment was carried out.

The time required for fracture reduction was measured. The robot movements and the reduction forces/moments